Sains Malaysiana 55(7)(2026): 1161-1172
http://doi.org/10.17576/jsm-2026-5507-05

Anti-inflammatory Constituents from *Bupleurum chinense* DC. Aerial Parts: Identification and Computational Mechanistic Insights

(Juzuk Anti-radang daripada *Bupleurum chinense* DC. Bahagian Aerial: Pengenalpastian dan Pemerhatian Mekanistik Pengiraan)

YUNAN SUN[1,2], YINGYING SHI[1,2], XUEGUI LIU[1,3,4], PINYI GAO[2,4] & DANQI LI[1,3,4,*]

[1]*Institute of Functional Molecules, Shenyang University of Chemical Technology, Shenyang, Liaoning 110142, PR China*
[2]*School of Chemical Engineering, Shenyang University of Chemical Technology, Shenyang, Liaoning 110142, PR China*
[3]*Liaoning Province Key Laboratory of Green Functional Molecular Design and Development, Shenyang University of Chemical Technology, Shenyang 110142, PR China*
[4]*National-Local Joint Engineering Laboratory for Development of Boron and Magnesium Resources and Fine Chemical Technology, Shenyang University of Chemical Technology, Shenyang 110142, PR China*

Received: 12 March 2026/Accepted: 11 July 2026

ABSTRACT

Bupleurum chinense DC. is a medicinal plant used for inflammatory conditions. While the anti-inflammatory activity of its roots is well established and attributed to saikosaponins, its aerial parts are routinely discarded during processing, leaving their chemical composition and bioactivity largely unexplored. To address this, a systematic phytochemical and anti-inflammatory study were conducted on these abandoned aerial tissues. The 70% ethanol extract of aerial parts was fractionated through silica gel column chromatography, ODS reversed-phase chromatography and preparative HPLC, affording 16 compounds structurally characterized by NMR and HR-ESI-MS. These isolates were categorized into four major groups, including flavonoids (**6**, **7**), organic acids (**1-4**, **10-14**), terpenoids (**15**, **16**), lignans and sterols (**5**, **8**, **9**). Subsequent anti-inflammatory assays on LPS-stimulated RAW264.7 macrophages at concentrations of 6.25-100 μM showed that methyl chlorogenate exhibited the most potent inhibitory effect on NO production, superior to all other isolated constituents. This research expands the chemical constituent library of *B. chinense* aerial parts and identifies methyl chlorogenate as a promising anti-inflammatory lead compound, providing solid chemical and pharmacological evidence for the sustainable high-value utilization of the aerial waste resources of this medicinal plant.

Keywords: Anti-inflammatory activity; *Bupleurum chinense* DC; chemical constituents; computer simulation

ABSTRAK

Bupleurum chinense DC. ialah tumbuhan ubatan yang digunakan untuk keadaan keradangan. Walaupun aktiviti anti-radang akarnya telah terbukti dan dikaitkan dengan saikosaponin, bahagian atasnya secara rutin dibuang semasa pemprosesan, menyebabkan komposisi kimia dan bioaktivitinya sebahagian besarnya belum diterokai. Untuk menangani perkara ini, satu kajian fitokimia dan anti-radang yang sistematik telah dijalankan ke atas tisu atas yang terbiar ini. Ekstrak etanol 70% daripada bahagian atas telah dipecahkan melalui kromatografi turus gel silika, kromatografi fasa terbalik ODS dan HPLC preparatif, menghasilkan 16 sebatian yang dicirikan secara struktur oleh NMR dan HR-ESI-MS. Pencilan ini dikategorikan kepada empat kumpulan utama, termasuk flavonoid (**6, 7**), asid organik (**1-4, 10-14**), terpenoid (**15, 16**), lignan dan sterol (**5, 8, 9**). Ujian anti-radang seterusnya pada makrofaj RAW264.7 yang dirangsang oleh LPS pada kepekatan 6.25-100 μM mendedahkan bahawa metil klorogenat menunjukkan kesan perencatan yang paling kuat terhadap penghasilan NO, lebih baik daripada semua juzuk terpencil yang lain. Kajian ini memperluaskan perpustakaan juzuk kimia bahagian udara *B. chinense* dan mengenal pasti metil klorogenat sebagai sebatian plumbum anti-radang yang berpotensi, memberikan bukti kimia dan farmakologi yang kukuh untuk penggunaan sumber sisa udara tumbuhan ubatan ini yang bernilai tinggi dan mampan.

Kata kunci: Aktiviti anti-radang; *Bupleurum chinense* DC; juzuk kimia; simulasi komputer

INTRODUCTION

The genus *Bupleurum* L. (Apiaceae) comprises a remarkable diversity of species, with more than 248 documented worldwide. According to the *Flora of China*, this genus comprises 36 species, 17 varieties, and 7 forms in China, which are predominantly distributed across the plateaus of northwestern and southwestern China (Yang et al. 2017). Among these species, *B. chinense* occupies a particularly prominent position. Its dried root, referred to as 'Chai Hu' in the system of Traditional Chinese Medicine, has well-established clinical application for febrile conditions, inflammatory conditions, and hepatic disorders (Sun et al. 2019). While the roots have been extensively studied phytochemically and pharmacologically, leading to the identification of major active constituents including saikosaponins, flavonoids, lignans, the aerial parts (stems and leaves) remain largely unexplored and are often discarded as agricultural by-products. This underutilization represents a significant waste of biomass and a missed opportunity for discovering novel bioactive molecules (Yang et al. 2023). Given the distinct ecological functions and biosynthetic pathways often active in aerial tissues, it is hypothesized that the chemical profile of these parts may differ substantially from that of the roots, potentially harboring unique compounds with valuable biological activities. Initial investigations into *B. chinense* have indicated the occurrence of flavonoids and phenylpropanoids. These constituents have exhibited notable anti-neuroinflammatory activities in epileptic experimental models, which are believed to be exerted through inhibiting the TREM1/NF-κB, thus suppressing the release of pro-inflammatory mediators including NO, TNF-α, and IL-6 (Li et al. 2022). Moreover, oleanane-type triterpenoid saponins derived from the aerial portions of *B. chinense* var. *rotundifolium* have shown notable therapeutic efficacy in experimental models of chronic skin inflammation, further underscoring the pronounced anti-inflammatory bioactivity of the aerial parts of this taxon (Navarro et al. 2001). However, a systematic and comprehensive chemical characterization of the above-ground parts of *B. chinense*, together with a detailed evaluation of the anti-inflammatory activities of its individual components, is still lacking.

To address this knowledge gap and scientifically validate the potential for the value-added utilization of this resource, a detailed phytochemical investigation guided by chromatographic techniques is imperative. In this study, systematic bioactivity-guided isolation study on the 70% ethanolic extract of *B. chinense* was carried out. Sixteen compounds were successfully obtained and purified using modern chromatographic techniques including normal-phase silica gel column chromatography, reversed-phase ODS column chromatography and preparative high-performance liquid chromatography (preparative HPLC). Their structures were unambiguously clarified by comprehensive spectral analysis, primarily employing 1D and 2D NMR and HR-ESI-MS, which represent fundamental analytical approaches for structural identification in the natural product chemistry. Compounds were subsequently assessed for their anti-inflammatory capacity via determination of their suppressive effects on NO generation in LPS-activated RAW 264.7 cells. Molecular docking was employed to elucidate possible binding interactions between the bioactive constituents and major inflammatory target TNF-*α*, thereby offering preliminary insights into the underlying molecular mechanisms. This study aims not only to expand the chemical inventory of *B. chinense* but also to identify novel anti-inflammatory lead compounds from its underutilized aerial parts, thereby providing a scientific foundation for their sustainable exploitation.

EXPERIMENTAL DETAILS

REGENTS AND MATERIALS

Column chromatography was carried out with 200-300 mesh silica gel, and thin-layer chromatography was performed on pre-coated silica gel GF_{254} plates (Qingdao Aoda Chemical Co., Ltd., Qingdao, China). Other chromatographic materials included ODS-A-HG, MCI, YMC-pack ODS A, and Promosil C_{18}. HPLC analysis was conducted using a Shimadzu LC-6AD system equipped with an SPD-20A UV detector. NMR and HRMS data were obtained on a Bruker AVIII 600 MHz and an Agilent 6540 UHD Q-TOF mass spectrometer, respectively. RAW 264.7 cells were provided by the Cell Bank of the Chinese Academy of Sciences. LPS, NO, DMEM and FBS were purchased from Beyotime, Gibco and Thermo Fisher Scientific.

EXPERIMENTAL MATERIALS

The aerial parts (stems and leaves) of *B. chinense* were collected from Jilin City, Jilin Province, China, and authenticated by Prof. Jincai Lu. No. BCH-012 (voucher specimen) was deposited at the Institute of Functional Molecules, Shenyang University of Chemical Technology for future reference.

EXTRACTION AND PURIFICATION

B. chinense (30 kg) were subjected to three successive rounds of hot reflux extraction (2 h each) with 70% aqueous ethanol at 80 °C. The extracts were combined and concentrated evaporated at 50.0 °C, affording 7349.2 g of the crude ethanolic extract. The concentrated extract was suspended in water and partitioned with dichloromethane and *n*-butanol. Three dichloromethane extractions afforded 767.1 g of organic-phase extract. The remaining aqueous phase was then extracted three times with *n*-butanol to give 1828.1 g of extract. A total of sixteen compounds (designated as 1–16) were purified from the dichloromethane and n-butanol fractions through

an integrated multi-step chromatographic strategy combining silica gel column chromatography, ODS reversed-phase column chromatography and preparative HPLC. Subfractions containing single target components were finally purified by preparative HPLC on a C_{18} column (250 × 20 mm, 5 μm). The mobile phase consisted of methanol–water with gradient elution; the flow rate was set at 1.5 mL min^{-1}, injection volume (10 μL), and the detection wavelength was 254 nm. A schematic outline of the isolation procedure is provided in Figure S1 (data not shown).

NITRIC OXIDE (NO) ASSAY

To evaluate LPS-induced inflammation and the anti-inflammatory activity of target compounds, NO production in RAW 264.7 cells was measured via Griess reagent assay. Cells were seeded in complete DMEM supplemented with 10% fetal bovine serum and 1% penicillin-streptomycin solution, and incubated at 37 °C in a humidified incubator containing 5% CO_2 for 24 h to adhere stably. RAW 264.7 cells were seeded at 2 × 10^4 cells/well in 96-well plates and incubated for 24 h for attachment. After cell adherence, RAW264.7 macrophages were pretreated with gradient concentrations of isolated test compounds (6.25–100 μM) for 1 h, then stimulated with 1 μg/mL LPS for another 24 h to induce inflammatory inflammation. Blank control group (only medium) and LPS-model group (LPS stimulation without compound treatment) were set synchronously in this assay. After incubation, collect the cell supernatant. Follow the instructions of the Griess reagent kit for the operation: Take 50 μL of solutions of different concentrations of $NaNO_2$ (0, 1, 2, 5, 10, 20, 40, 60, 100 μM) as standards and add them to a 96-well plate. Take 50 μL of the supernatant and add it to another 96-well plate. Finally, add 50 μL of Griess reagent I (sulfanilic acid solution) and mix them. React at room temperature in the dark for 5 min. Then add 50 μL of Griess reagent II (N-1-naphthyl ethylenediamine hydrochloride solution) and continue to react in the dark for 5 min. Use an enzyme reader to measure the absorbance at a wavelength of 540 nm. Calculate the NO concentration based on the standard curve. Set 3 duplicate wells for each group experiment and take the average value as the final result. By comparing the NO release levels of different treatment groups, evaluate the degree of inflammation induced by LPS.

STATISTICAL ANALYSIS

Statistical evaluation was performed by one-way ANOVA combined with Dunnett's post hoc test using GraphPad Prism 10.0 software. Data are expressed as mean ± SD from three independent replicates, and a *p*-value of less than 0.05 was defined as statistically significant.

DOCKING STUDIES

TNF was obtained from the PDB, together with corresponding system preparation protocol. Firstly, PyMOL software was employed to remove water molecules, cofactors, and other irrelevant ligands from the crystal structure to ensure the purity of the protein model. Hydrogen atoms were added and protonation states were optimized to refine the physicochemical properties of the protein. The two-dimensional structure of compound **1** was obtained from the PubChem database and subsequently prepared for docking. The ligand was first converted from 2D to 3D format, energy-minimized, and then saved in PDB format to serve as a high-quality input for docking simulations. Molecular docking analysis were implemented utilizing the AutoDock Vina package. The preprocessed protein and ligand structures were imported, and docking calculations were conducted with defined search parameters. The software systematically explores possible binding conformations of the ligand within the protein's active site and estimates the binding free energy for each pose. Upon completion, docking output provides data including binding free energies, predicted binding conformations, and interaction details.

RESULTS

STRUCTURAL IDENTIFICATION

Compounds **2-3** and **5-16** were isolated for the first time from the aerial parts of plants belonging to the genus *B. chinense* for the first time. Their chemical classifications are as follows: compounds **1**, **2**, **3**, **4**, **10**, **11**, and **12** are organic acids and their esters; compounds **6** and **7** are flavonoid; compounds **5** and **8** belong to the lignan class; compounds **15** and **16** are terpenes; compound **14** is a phenylpropanoid derivative; and compounds **9** and **13** are aromatic compounds.

Methyl chlorogenate **(1)**, yellow oil, exhibited a chemical formula of $C_{17}H_{20}O_9$ by HRESIMS, m/z 391.1006 ($[M+Na]^+$, calcd for 391.1005) (Figure S2.3 - data not shown). ^1H NMR at δ_H 7.55 (d, J = 15.8 Hz, H-7′ C=C) and 6.24 (d, J = 15.8 Hz, H-8′ C=C). Aromatic proton signals corresponding to the benzene ring were observed at δ_H 7.08 (s, H-2′), 6.97 (d, J = 7.7 Hz, H-6′), 6.81 (d, J = 7.7 Hz, H-5′). Protons of the six-membered ring were detected at δ_H 5.31 (s, H-3), 4.17 (m, H-5), 3.78 (m, H-4), and 2.04–2.24 (m, H-2, 6). A methoxy group signal appeared at δ_H 3.73 (s, 7-OCH_3) (Figure S2.1 - data not shown). ^{13}C NMR data enabled the assignment of all carbons, which were categorized as follows: two sets of olefinic carbons at δ_C 176.3, 169.2, 150.5, and 115.9; aromatic carbons belonging to the benzene ring at δ_C 148.1, 147.7, 128.5, 123.9, 117.4, and 116.0; two oxygenated carbons at δ_C 69.5 and 78.5; six-membered

ring carbons at δ_C 76.8, 73.5, 72.8, 71.3, 38.9, and 38.8; as well as one methoxy carbon at δ_C 53.9 (Figure S2.2 - data not shown). The data were basically consistent with the reports in Li et al. (2024).

Methyl-5-*O*-*p*-coumaroylquinic acid **(2)**, yellow oil, was established as $C_{17}H_{20}O_8$. ^{1}H NMR δ_H 7.63 and 6.31. Aromatic proton signals attributable to the benzene ring were observed at δ_H 7.47 (d, J = 8.6 Hz, H-2′, 6′), 6.82 (d, J = 8.6 Hz, H-3′, 5′). Signals corresponding to protons of the six-membered ring were detected at δ_H 4.17 (m, H-3), 3.76 (m, H-4), 5.31 (m, H-5) and 2.02–2.25 (m, H-2, 6). Additionally, a methoxy proton signal appeared at δ_H 3.72 (s, 7-OCH$_3$) (Figure S3.1 - data not shown). ^{13}C NMR showed assignable carbons corresponding to specific functional groups and structural fragments: δ_C 176.3(C=O), a methoxy carbon at δ_C 53.8, a carbonyl carbon at δ_C 169.1, aromatic carbons at δ_C 162.3, 132.8, 127.9, 117.7, and six-membered ring carbons at δ_C 76.7, 73.5, 73.0, 71.2, 38.9, 37.4 (Figure S3.2 - data not shown). The data were basically consistent with the reports in Fan et al. (2025).

(-)-5-*O*-feruloylquinic acid methyl ester **(3)**, yellow oil, exhibited a chemical formula of $C_{18}H_{22}O_9$ by HRESIMS, at m/z 405.1165 ([M+Na]$^+$, calcd for 405.1162) (Figure S4.3 - data not shown). ^{1}H NMR δ_H 7.61 (d, J = 15.9 Hz, H-7′, C=C) , 6.34 (d, J = 15.9 Hz, H-8′, C=C), benzene ring protons at δ_H 7.20 (d, J = 1.7 Hz, H-2′), 7.10 (dd, J = 1.7, 8.2 Hz, H-6′), 6.84 (d, J = 8.2 Hz, H-5′), six-membered ring protons at δ_H 5.32 (m, H-5), 4.17 (m, H-3), 3.76 (m, H-4), 2.16 (m, H-2), 2.05 (m, H-6), δ_H 3.91 (s, 3′-OCH$_3$), ester group protons at δ_H 3.72 (s, -COOCH$_3$) (Figure S4.1 - data not shown). ^{13}C NMR spectrum exhibited carbon resonances assignable to distinct structural moieties, including carbonyl carbon at δ_C 176.3 (C=O) and 169.1, aromatic carbons at the benzene ring at δ_C 151.6, 150.2, 147.9, 128.4, 125.0, 117.4, 116.2, and 112.5, as well as two sets of six-membered ring carbons at δ_C 76.8, 73.5, 72.9, 71.3, 38.9, and δ_C 76.7, 73.5, 73.0, 71.2, 38.9, 37.4. Additionally, methoxy carbon at δ_C 57.3 and ester carbon at δ_C 53.8 were observed (Figure S4.2 - data not shown). The data were basically consistent with the reports in Asamenew et al. (2019).

(-)-5-*O*-feruloylquinic acid butyl ester **(4)**, yellow oil, was elucidated to possess the molecular formula $C_{20}H_{28}O_9$ by HRESIMS, m/z 411.1665 ([M−H]$^-$, calcd for 411.1655) (Figure S5.3 - data not shown). ^{1}H NMR showed two *trans*-configured olefinic protons at δ_H 7.64 (d, J = 15.9 Hz, H-7′) and 6.34 (d, J = 15.9 Hz, H-8′); three aromatic protons of the benzene ring at δ_H 7.21 (s, H-2′), 7.10 (dd, J = 1.2, 8.1 Hz, H-6′), and 6.84 (d, J = 8.1 Hz, H-5′); five protons belonging to the six-membered ring at δ_H 5.31 (m, H-5), 4.13 (m, H-3), 2.23 (m, H-4), 2.16 (m, H-2), and 2.05 (m, H-6); a *n*-butyl group at δ_H 3.77 (dd, J = 3.06, 3.05 Hz, H-8), 1.65 (m, H-9), 1.38 (m, H-10), and 0.93 (t, H-11), one methoxy group at δ_H 3.92 (s, -OCH$_3$) (Figure S5.1 - data not shown). ^{13}C NMR spectrum displayed characteristic carbon signals corresponding to different structural units: carbonyl carbons at δ_C 175.9 and 169.1; aromatic carbons of the benzene ring at δ_C 151.7, 150.3, 148.0, 128.4, 125.0, 117.4, 116.3, and 112.5; five carbons belonging to the six-membered ring at δ_C 76.7, 73.4, 73.1, 71.2, and 38.9; a methoxy carbon at δ_C 57.3; as well as carbons of the *n*-butyl group at δ_C 67.2, 32.5, 21.0, and 14.9 (Figure S5.2 - data not shown). The data were basically consistent with the reports in Takara et al. (2002).

(+)-isolariciresinol-3α-*O*-β-D-glucopyranoside **(5)**, white powder, was assigned the molecular formula $C_{26}H_{34}O_{11}$ by HRESIMS, m/z 545.2001 ([M+Na]$^+$, calcd for 545.1999) (Figure S6.3 - data not shown). ^{1}H NMR showed three aromatic protons at δ_H 6.82 (d, J = 1.8 Hz, H-2′), 6.77 (d, J = 8.0 Hz, H-5′), and 6.66 (d, J = 1.9 Hz, H-6′), together with two isolated aromatic protons at δ_H 6.68 (s, H-8) and 6.21 (s, H-5); two methoxy groups at δ_H 3.84 (s, 7-OCH$_3$) and 3.83 (s, 3′-OCH$_3$); protons of the glycosidic chain at δ_H 4.15 (d, J = 7.8 Hz, H-1″), 3.70-3.77 (m, H-6″), and 3.20-3.26 (m, partly overlapped); as well as aliphatic protons at δ_H 2.84-2.86 (m, H-1a, H-1b), 2.11-2.23 (m, H-3), and 1.90–2.07 (m, H-2) (Figure S6.1 - data not shown). ^{13}C NMR spectrum displayed characteristic carbon signals corresponding to distinct structural moieties: aromatic carbons at δ_C 149.7, 148.0, 146.7, 146.0, 139.5, 135.3, 130.0, 124.0, 118.3, 116.9, 115.1, and 113.3; carbons of the glycosidic chain at δ_C 106.1, 79.0, 78.8, 76.1, 72.5, and 63.6; aliphatic carbons belonging to the heterocyclic ring at δ_C 70.3 and 66.0; two methoxy carbons at δ_C 57.3 and 57.2; as well as saturated aliphatic carbons at δ_C 48.8, 46.8, 40.4, and 34.8 (Figure S6.2 - data not shown). The data essentially matches the results reported in Wen et al. (2012).

5,7,3’,4’-tetrahydroxy-4’’-*O*-methyl-3-*O*-β-d-glucopyranosideflavonol **(6)** obtained as a yellow crystalline powder. Its molecular formula was determined to be $C_{22}H_{22}O_{12}$ via HRESIMS analysis, which gave a sodiated molecular ion peak at m/z 501.1014 ([M+Na]$^+$; calculated value = 501.1009) (Figure S7.3 - data not shown). ^{1}H NMR spectrum displayed proton resonances corresponding to various structural units: three aromatic protons of the benzene ring at δ_H 7.74 (d, J = 2.1 Hz, H-2′), 7.62 (dd,J = 2.1, 8.9 Hz, H-6′), and 6.90 (d, J = 8.9 Hz, H-5′); two isolated aromatic protons at 6.23 (s, H-6),δ_H 6.42 (s, H-8); protons of the glycosidic chain at δ_H 5.28 (d, J = 7.7 Hz, H-1″), 3.50 (m, H-2″), 3.46 (m, H-3″), 3.36 (m, H-4″), 3.26 (m, H-5″), and 3.75 (m, H-6″), δ_H 3.61 (s, -OCH$_3$) (Figure S6.1 - data not shown). ^{13}C NMR spectrum presented the carbon signals corresponding to distinct structural fragments: twelve aromatic carbons from two benzene rings at δ_C 180.3, 167.0, 163.9, 159.9, 159.4, 136.5, 150.7, 146.8, 124.0, 123.9, 118.4, and 118.9; three non-protonated aromatic carbons at δ_C 106.5, 100.8, and 95.6; carbons of the glycosidic chain at δ_C 105.2, 79.3, 79.0, 76.6, 72.1,

and 63.4; as well as one methoxy carbon at δ_C 50.4 (Figure S7.2 - data not shown). The spectroscopic data obtained herein correspond well to those documented in Liao, Liu and Yuan (2012).

β-D-fructfuranosyl-*α*-D-(6-vanilloyl)-glucopyranoside **(7)**, obtained as a yellow powder, this compound was determined to have the molecular formula $C_{20}H_{28}O_{14}$ using HRESIMS. The ^{1}H NMR spectrum demonstrated three aromatic protons of the benzene ring at δ_H 7.74 (d, J = 2.1 Hz, H-2′), 7.62 (dd, J = 2.1, 8.9 Hz, H-6′), and 6.90 (d, J = 8.9 Hz, H-5′); two singlet aromatic protons at δ_H 6.42 (s, H-8) and 6.23 (s, H-6); protons corresponding to the glycosyl chain at δ_H 5.28 (d, J = 7.7 Hz, H-1″), 3.50 (m, H-2″), 3.46 (m, H-3″), 3.36 (m, H-4″), 3.26 (m, H-5″), and 3.75 (m, H-6″), δ_H 3.61 (s, -OCH$_3$) (Figure S8.1 - data not shown). Analysis of the ^{13}C NMR spectrum showed a set of carbon resonances consistent with the proposed structure. These included six aromatic carbons (encompassing two benzene ring systems) at δ_C 154.5, 149.8, 126.0, 122.9, 117.0, and 114.3, and a downfield ester carbonyl carbon at δ_C 169.6. The anomeric and ring carbons of the sugar unit were identified at δ_C 106.2, 94.5, 84.7, 80.1, 76.6, 75.5, 75.2, 74.0, 72.2, 64.9, 64.2, and 63.1, with a methoxy carbon signal further observed at δ_C 57.2 (Figure S8.2 - data not shown). The spectroscopic data obtained herein corresponds to those documented in Takara et al. (2002).

Isolariciresinol **(8)** obtained as a white powder, was found the molecular formula $C_{20}H_{24}O_6$ by HRESIMS, where the experimental mass for the sodium adduct ion ([M+Na]$^+$, m/z 383.1468) was in excellent agreement with the calculated value of 383.1471 (Figure S9.3 - data not shown). ^{1}H NMR spectrum allowed the identification of diagnostic proton resonances associated with different structural units: aromatic protons from two benzene rings at δ_H 6.76 (d, J = 8.0 Hz, H-5′), 6.70 (d, J = 13.5 Hz, H-2′), 6.65 (s, H-8), 6.64 (s, H-6′), and 6.21 (s, H-5), δ_H 3.82 (s, 7-OCH$_3$) and 3.70 (s, 3′-OCH$_3$); together with protons of the six-membered carbocyclic ring at δ_H 3.67 (s, H-2a), 3.68 (s, H-3a), 3.42 (dd, J = 10.8, 3.5 Hz, H-2a), 2.80 (d, J = 7.7 Hz, H-1), 2.02 (m, H-2), 1.79 (t, H-3), and 3.82 (d, J = 18.6 Hz, H-4) (Figure S9.1 - data not shown). Analysis of the ^{13}C NMR spectrum showed characteristic carbon resonances associated with different structural units, including twelve aromatic carbons of two benzene rings at δ_C 149.9, 148.1, 146.8, 146.1, 139.5, 135.0, 129.9, 124.1, 118.2, 116.8, 114.6, and 113.2, two methylene carbons at δ_C 66.8 and 63.1, three carbons of the six-membered carbocyclic ring at δ_C 48.9, 40.8, and 34.4, together with two methoxy carbons at δ_C 57.2 and 57.1 (Figure S9.2 - data not shown). The spectroscopic data obtained herein corresponds well to those documented in Pel et al. (2022).

Fendleryl B **(9)**, a brown solid with the molecular formula of $C_{19}H_{14}O_6$ by HRESIMS, which exhibited at m/z 339.0866 ([M+H]$^+$, calcd for 339.0869) (Figures S10.3 - data not shown). ^{1}H NMR spectrum showed aromatic protons of benzene rings at δ_H 7.89 (d, J = 9.0 Hz, H-2, 6), 6.87 (d, J = 9.0 Hz, H-3, 5), 7.57 (d, J = 9.0 Hz, H-2″, 6″), and 6.84 (d, J = 9.0 Hz, H-3″, 5″), and a methoxy substituent at δ_H 57.3 (-OCH$_3$) (Figure S10.1 - data not shown). ^{13}C NMR spectrum showed ten aromatic carbons from two benzene ring systems at δ_C 169.5, 164.4, 153.7, 149.6, 133.6, 125.9, 123.0, 117.0, 116.8, and 114.4, as well as a methoxy carbon signal at δ_C 57.3 (Figure S10.2 - data not shown). The results are generally consistent with the data from Intaraudom et al. (2017).

Methyl shikimate **(10)**, a brown oily residue, and its molecular formula was established as $C_8H_{12}O_5$. ^{1}H NMR spectrum permitted the identification of diagnostic proton resonances associated with distinct structural moieties. Protons belonging to the six-membered ring were observed at δ_H 6.82 (s, H-2), 4.40 (m, H-3), 4.02 (m, J = 12.1, 5.4 Hz, H-5), 3.70 (dd, J = 7.0, 4.1 Hz, H-4), 2.73 (m, H-6a), and 2.23 (m, H-6b), in addition to a characteristic singlet attributable to the methyl ester group at δ_H 3.79 (s, -COOCH$_3$) (Figure S11.1 - data not shown). ^{13}C NMR spectrum showed characteristic carbon resonances corresponding to the six-membered ring system at δ_C 131.0, 140.0, 69.2, 68.1, 73.4, 32.3, and 169.5, together with a carbon signal arising from the ester methyl carbon at δ_C 51.0 (Figure S11.2 - data not shown). The data are basically consistent with those reported in Shrestha et al. (2013).

Methyl-2,4,6-trihydroxybenzoate **(11)**, isolated as colorless crystals, was characterized as having the molecular formula of $C_8H_8O_5$. ^{1}H NMR spectrum exhibited the proton signals of a benzene ring at δ_H 5.88 (s, H-3, 5) and methoxyl signal at δ_H 4.00 (s, -OCH$_3$) (Figure S12.1 - data not shown). ^{13}C NMR spectrum exhibited carbon resonances assignable to distinct structural moieties: aromatic carbons of benzene ring at δ_C 167.0, 164.8, 97.4, 95.0, 58.3 and carbonyl signal at δ_C 172.5 (Figure S12.2 - data not shown). The results are generally consistent with the data from Conradt et al. (2016).

(2'R)-phaselic acid **(12)**, a yellow amorphous powder, was elucidated to the molecular formula of $C_{13}H_{12}O_8$. The ^{1}H NMR spectrum exhibited diagnostic proton signals attributable to various structural moieties for structural identification. Aromatic signals of the benzene ring were observed at δ_H 7.07 (s, H-2), 6.97 (d, J = 1.9 Hz, H-6), and 6.81 (d, J = 8.2 Hz, H-5); olefinic protons were detected at δ_H 6.23 (d, J = 15.9 Hz, H-8) and 7.54 (d, J = 15.9 Hz, H-7), δ_H 5.30 (t, J = 4.4 Hz, H-2′ -CH$_2$-) and 3.72 (m, H-3′ -CH$_2$-) (Figure S13.1 - data not shown). ^{13}C NMR showed characteristic carbon signals assignable to the respective structural fragments: aromatic carbons of the benzene ring at δ_C 128.5, 116.0, 150.6, 147.7, 117.4, and 123.8; olefinic carbons at δ_C 148.1 and 115.9;

an ester carbonyl carbon at δ_C 180.0; a carboxyl carbon at δ_C 169.1; and methylene carbons at δ_C 73.0 and 38.9 (Figure S13.2 - data not shown). The data are basically consistent with the reports in Tazaki et al. (2002).

p-hydroxybenzaldehyde **(13)** was a white solid, and its molecular formula was $C_7H_6O_2$ by HRESIMS, m/z 177.0160 ([M+Na]$^+$, calcd for 177.0164) (Figure S14.3 - data not shown). Diagnostic proton resonances matching various structural moieties were observed in the ^{1}H NMR spectrum. Aromatic protons of the benzene ring were observed at δ_H 7.45 (s, H-2), 7.44 (s, H-6), and 6.82 (d, J = 8.4 Hz, H-5), together with a characteristic aldehyde proton signal at δ_H 9.77 (s, -CHO) (Figure S13.1 - data not shown). ^{13}C NMR spectrum exhibited aromatic carbons of the benzene ring at δ_C 152.7, 147.1, 124.5, 123.3, 118.2, and 116.7, as well as the carbon resonance of the carbonyl group at δ_C 193.6 (Figure S14.2 - data not shown). The current data match well with those described in Que, Dai and Huang (2009).

Dimethylcaffic acid **(14)**, isolated as white powder, was established to possess the molecular formula of $C_{11}H_{12}O_4$. Analysis of the ^{1}H NMR spectrum enabled the detection of characteristic proton signals linked to various structural fragments. Aromatic and olefinic protons were observed at δ_H 7.65 (d, J = 15.6 Hz, H-7), 7.21 (d, J = 1.8 Hz, H-2), 7.09 (dd, J = 1.8, 8.4 Hz, H-6), 6.83 (d, J = 8.4 Hz, H-5), and 6.37 (d, J = 15.6 Hz, H-8), δ_H 3.92 (s, 3-OCH_3) and 3.79 (s, 4-OCH_3) (Figure S15.1 - data not shown). The analysis of the ^{13}C NMR spectrum showed characteristic carbon resonances assignable to the respective structural fragments: aromatic carbons of the benzene ring at δ_C 128.4, 112.5, 150.3, 151.7, 116.0, and 125.0; olefinic carbons at δ_C 147.7 and 117.4; as well as carbon signals corresponding to two methoxy substituents at δ_C 57.3 and 52.9 (Figure S15.2 - data not shown). The data are basically consistent with the reports in Deng et al. (2024).

Saniculamoid D **(15)**, isolated as a white solid powder, was assigned the molecular formula $C_{14}H_{22}O_2$ by HRESIMS, m/z 245.1515 ([M+Na]$^+$, calcd for 245.1517) (Figure S16.3 - data not shown). The ^{1}H NMR spectrum showed proton signals characteristic of each structural moiety. Protons associated with the five-membered ring systems were observed at δ_H 2.67 (m, H-8a), 2.60 (m, H-8b), 2.16 (dd, H-1a), 2.04 (m, H-1b), 2.08 (m, H-2), 1.64 (dd, H-4), 0.70 (m, H-6a), 1.73 (m, H-7a), 1.66 (m, H-7b), 2.54 (m, H-8), 1.87 (m, H-10). Three methyl groups were detected at δ_H 1.78 (m, H-11), 1.06 (ddd, H-5), 0.96 (d, J = 5.4 Hz, H-12), 0.95 (d, J = 6.0 Hz, H-13), 2.18 (s, H-14), and 0.77 (m, H-6) (Figure S16.1 - data not shown). ^{13}C NMR spectrum exhibited carbons belonging to the five-membered ring at δ_C 30.7, 36.5, 218.6, 34.5, and 24.7, together with three methyl carbon resonances at δ_C 212.7, 48.5, 43.1, 33.3, 32.6, 30.4, 21.0, 20.4, and 26.6 (Figure S16.2 - data not shown). The data are basically consistent with the reports in Wang et al. (2018).

1β,6α-dihydroxyeudesma-4(15)-ene **(16)** isolated as oil, was determined to be $C_{15}H_{26}O_2$ by HRESIMS ([M+Na]$^+$ m/z 261.1824, calcd for 261.1830) (Figure S17.3 - data not shown). The ^{1}H NMR spectrum facilitated the identification of diagnostic proton resonances attributable to the distinct structural moieties. Protons of the six-membered ring systems were observed at δ_H 4.97 and 4.76 (s, H-15), 3.66 (t, J = 9.6 Hz, H-6), 3.36 (dd, J = 4.8, 12.0 Hz, H-1), 2.30 (H-3a and H-11), 2.09 (m, J = 4.8, 13.8 Hz, H-3b), 1.96 (d, J = 12.6 Hz, H-9a), 1.82 (m, H-2a), 1.75 (d, J = 10.2 Hz, H-5), 1.58 (m, H-2b and H-8a), 1.33 (m, H-7 and H-8b), 1.12 (m, J = 4.2, 24.6 Hz, H-9b), 0.95 (d, J = 7.0 Hz, H-12), 0.88 (d, J = 7.2 Hz, H-13), and 0.71 (H-14, s) (Figure S17.1 - data not shown). ^{13}C NMR spectrum showed characteristic carbon resonances assignable to the six-membered ring skeleton at δ_C 147.6, 109.9, 80.7, 68.9, 57.4, 52.6, 43.8, 38.4, 37.3, 33.7, 27.8, 22.5, 20.2, 17.2, and 13.0 (Figure S17.2 - data not shown). The data are basically consistent with the reports in Yang et al. (2018).

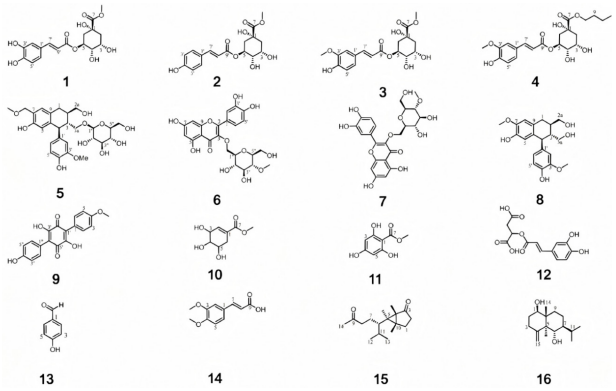

CELL VIABILITY

MTT experiment with LPS and compounds

A preliminary MTT-based cytotoxicity screening was conducted to identify suitable LPS concentrations for cell model establishment. No marked cytotoxicity was observed across the 0.25-4 μg/mL range, with cell viabilities recorded as 95.8%, 98.7%, 97.9%, 97.2%, and 96.9%, respectively. Hence, 0.5, 1, and 2 μg/mL LPS were chosen for inflammation induction, prioritizing minimal impact on cell viability while ensuring effective stimulation. Subsequently, the cytotoxicity of all 16 compounds (**1-16**) was evaluated on RAW 264.7 macrophages using the MTT assay across a concentration range of 6.25, 12.5, 25, 50, and 100 μM. As summarized in Figure S2 (data not shown), based on the criterion of cell viability ≥ 80%, non-cytotoxic concentrations were selected for each compound in the subsequent LPS-induced NO inhibition assays. This ensures that the observed anti-inflammatory effects are not confounded by compound-induced cell death.

Selection of optimal LPS concentration for inflammation induction

To establish an *in vitro* inflammatory model, nitric oxide (NO) release was quantified following LPS treatment. As shown in Figure 1, NO production in the untreated control group was 2.9 μM. In contrast, stimulation with 0.5 μg/mL LPS-elicited a significant elevation in NO release to 23.9 μM, confirming its potent pro-inflammatory effect. Interestingly, NO levels at higher LPS concentrations of 1 and 2 μg/mL were 20.9 μM and 19.1 μM, respectively, which were lower than that induced by 0.5 μg/mL. Collectively, the results from the MTT assay and NO content determination indicated that 0.5 μg/mL is the optimal LPS concentration for inducing inflammation in subsequent experiments.

LPS-induced NO inhibitory activity

Building on the significant anti-inflammatory action exerted by the crude extract, the NO production of 16 isolated compounds was further determined to evaluate their inhibitory effects on LPS-induced inflammatory responses. As illustrated in Figure 2, stimulation with 0.5 μg/mL LPS significantly elevated NO release to 32.9 μM compared to the basal level of 3.6 μM in the untreated control group, confirming a robust inflammatory state. Among the 16 tested compounds, the NO levels in compound-treated groups were attenuate in the LPS-treated group, indicating that all these compounds possess certain anti-inflammatory potential. Notably, compound **1**, a caffeoylquinic acid derivative structurally related to cynarin and isochlorogenic acids, exerted significant anti-inflammatory activity across all tested concentrations (6.25-100 μM) (Zhang et al. 2018). The NO levels were reduced to 8.2, 7.5, 7.8, 6.3, and 6.0 μM, respectively, demonstrating a concentration-dependent inhibitory effect. This observation aligns with the well-documented anti-inflammatory properties of caffeoylquinic acid derivatives, which have been reported to suppress iNOS expression and NF-κB activation in LPS-activated macrophages (Liu et al. 2021; Torres-Rodríguez et al. 2016). Among all tested compounds, compound **14** exhibited the most potent NO inhibitory activity. At 100 μM, it reduced NO production to 4.5 μM, approaching the level of the unstimulated normal control group (3.8 ± 0.5 μM), suggesting near-complete suppression of LPS-induced inflammatory activation. This potency is comparable to that of saikosaponin D, a well-characterized anti-inflammatory constituent of *B. chinense* known to exert its effects via NF-κB and MAPK pathway modulation (Ma et al. 2015; Park et al. 2015; Yan et al. 2024). Compounds **4**, **6**, and **10** also demonstrated favorable activity at 100 μM, with NO release levels of 9.0, 7.8, 4.2, and 8.8 μM, respectively. The differential potency among these structurally related compounds suggests a structure-dependent activity profile, which may be attributed to variations in glycosylation patterns or substitution positions on the flavonoid/saponin (Li, Pan & Xu 2019; Yang et al. 2025). Compound **15**, a terpenoid constituent, the NO concentration was determined to be 9.0 μM at 100 μM, confirming its moderate yet consistent anti-inflammatory potential. Compounds **3**, **5**, **7**, and **9** displayed moderate inhibition, maintaining NO levels below 20 μM across all tested concentrations with a tentative concentration-dependent trend. Collectively, the dose-dependent suppression of NO production by compounds **1**, **14**, and **15** provided molecular-level evidence supporting their potential as bioactive equivalents contributing to the anti-inflammatory effects of *B. chinense* (Zhao et al. 2025). Regarding the active compound **15** (Saniculamoid D), the NO concentration was determined to be 9.0 μM at a dosage of 100 μM, which was lower than that in the LPS-stimulated group. Compounds **3**, **5**, **7**, and **9** exhibited moderate inhibition, maintaining NO levels below 20 μM across all tested concentrations while showing a tentative concentration-dependent trend.

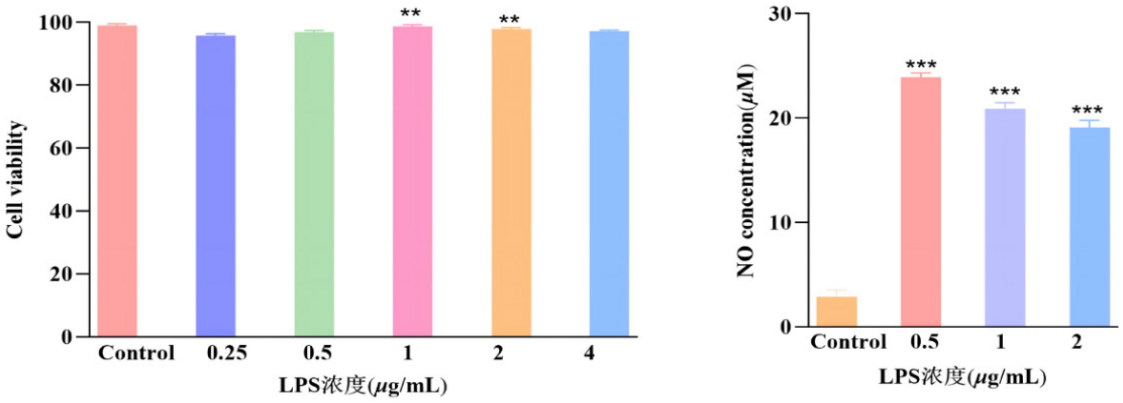

FIGURE 1. The MTT and NO experiment of LPS on RAW264.7 cells

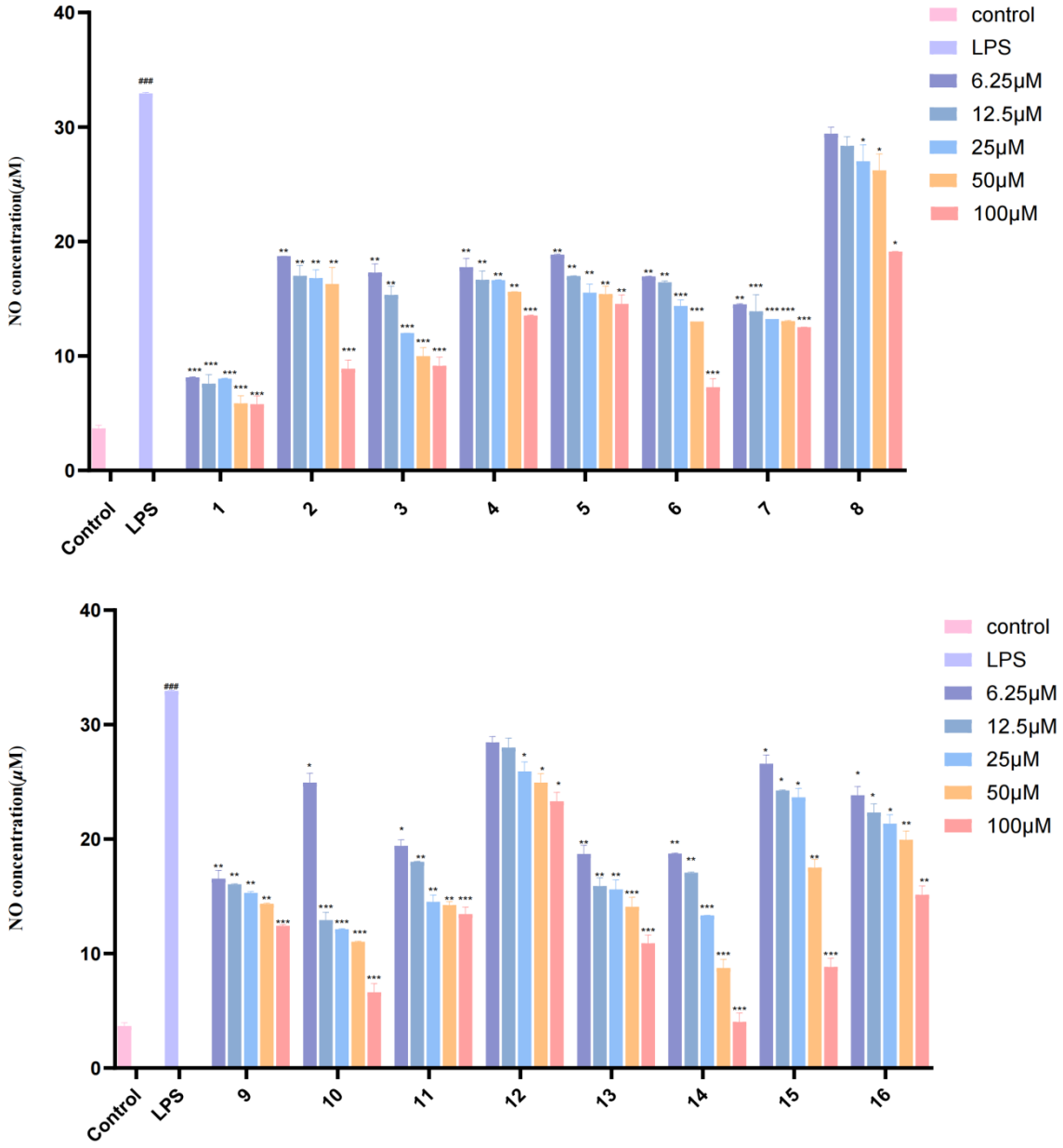

FIGURE 2. Determination of NO Content in compounds **1-16**

Molecular docking results

The core objective is to screen all compounds that can bind to the target in order to verify the experimental results. Binding energy is a key indicator for evaluating the stability of the receptor-ligand binding. The lower the binding energy in the docking process, the more stable the binding is. Generally, a binding energy of < -5 kcal/mol indicates strong binding activity. Given its potent anti-inflammatory activity and TNF-α targets with good anti-inflammatory activity were selected for molecular docking verification. The results show that the binding energy of compound **1** with TNF-α is -8.0 kcal/mol. The target compound binds to the active cavity of the receptor and participates in molecular recognition through hydrogen bonds and van der Waals forces. The aromatic ring system achieves hydrophobic binding through Pi-alkyl interactions. These typical non-covalent interaction patterns effectively maintain the structural stability of the complex, indicating that the ligand has a high binding affinity with the target protein. According to the molecular docking results, as shown in Table 1, target protein TNF-*α* have good binding with **16** compounds, respectively. The represented results of molecular docking are visualized in three- and two-dimensional structural models (Figure 3).

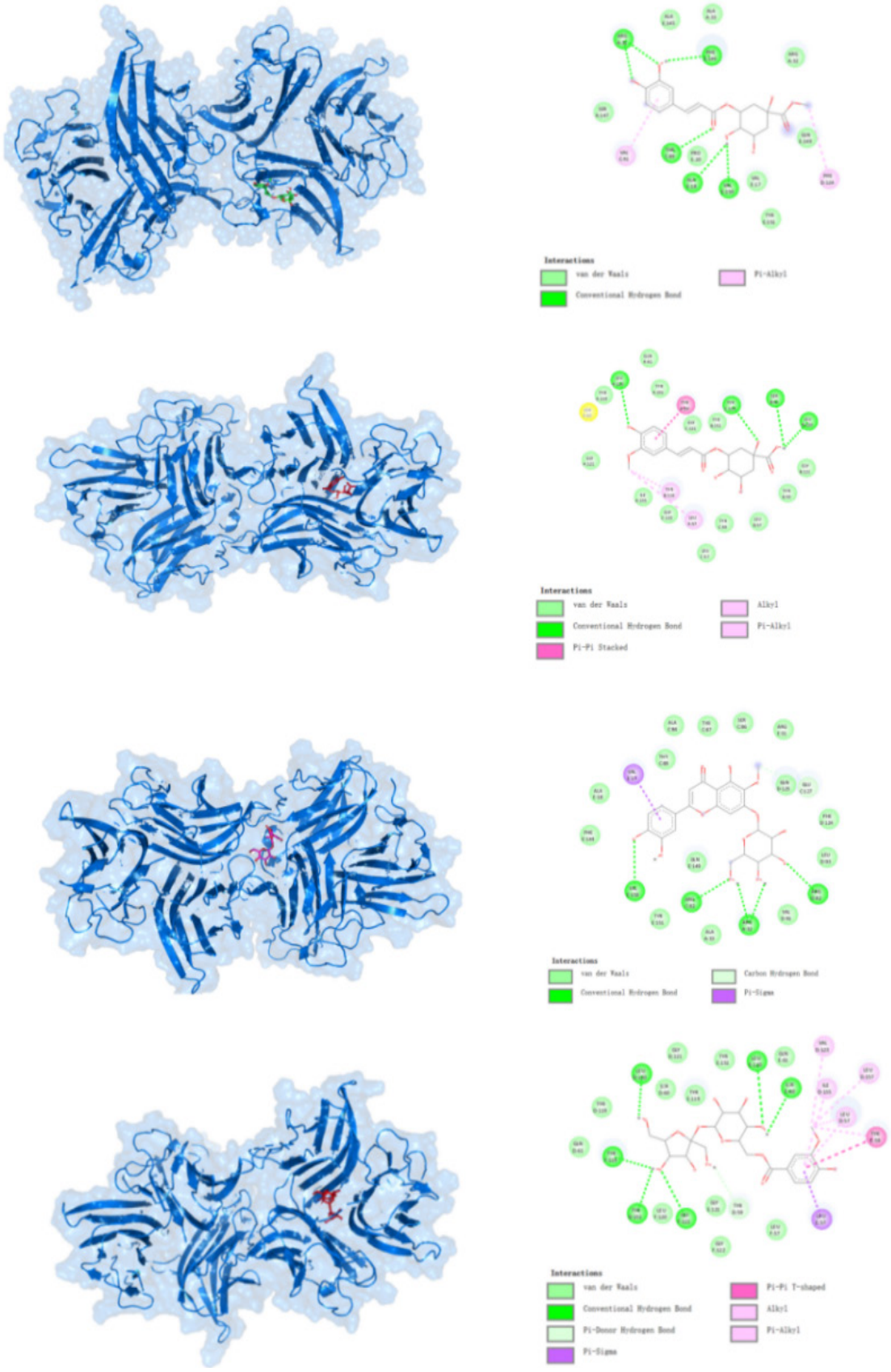

FIGURE 3. Docking diagram of compounds **1**, **4**, **6**, **7** with TNF-α target

TABLE 1. The molecular docking results of the TNF-α targets with compounds

Compound	Affinity(kcal/mol)
Methyl chlorogenate (**1**)	-8.0
Methyl-5-*O*-*p*-coumaroylquinic acid (**2**)	-9.4
(-)-5-*O*-feruloylquinic acid methyl ester (**3**)	-6.6
(-)-5-*O*-feruloylquinic acid butyl ester (**4**)	9.4
(+)-isolariciresinol-3*α*-*O*-*β*-D-glucopyranoside (**5**)	-8.5
5,7,3',4'-tetrahydroxy-4''-*O*-methyl-3-*O*-*β*-d-glucopyranosideflavonol (**6**)	-9.1
β-D-fructfuranosyl-*α*-D-(6-vanilloyl)-glucopyranoside (**7**)	-8.9
Isolariciresinol (**8**)	-8.5
Fendleryl B (**9**)	-7.8
Methyl shikimate (**10**)	-6.5
Methyl-2,4,6-trihydroxybenzoate (**11**)	-6.7
(2'R)-phaselic acid (**12**)	-8.2
P-hydroxybenzaldehyde (**13**)	-5.8
Dimethylcaffic acid (**14**)	-7.4
Saniculamoid D (**15**)	-5.9
1*β*,6*α*-dihydroxyeudesma-4(15)-ene (**16**)	-8.7

DISCUSSION

Traditional pharmacopeias and modern research on *B. chinense* have predominantly focused on its roots, which are rich in bioactive saikosaponins and form the basis of its well-documented hepatoprotective and anti-inflammatory uses. This root-centric approach has, however, led to the relative neglect of its aerial parts as a potentially a promising source of novel bioactive constituents (Sun et al. 2019). Consequently, the chemical profile and therapeutic potential of these non-traditional plant parts remain substantially underexplored, representing a significant gap in knowledge and a possible underutilization of the plant's full medicinal resource. Our study directly addresses this imbalance by systematically investigating the chemical constituents of *B. chinense*. In the present study, **16** compounds were isolated and identified from *B. chinense*, which enriches the chemical profile of the genus *B. chinense.* More importantly, this work provided clear phytochemical evidence delineating the distinct compositional landscape of the aerial parts from the saikosaponin-dominated roots, thereby repositioning the aerial biomass not as a byproduct but as a unique reservoir of potentially valuable secondary metabolites worthy of separate pharmacological evaluation.

In the bioactivity screening, methyl chlorogenate (compound **1**) was identified as the most promising anti-inflammatory constituent. It demonstrated a potent and concentration-dependent inhibitory effect on NO production in LPS-stimulated RAW 264.7 macrophages across the tested range (6.25-100 μM). It is a methylated derivative of chlorogenic acid, shows a highly structural similarity with chlorogenic acid, differing only at the carboxyl terminus. Research has demonstrated that chlorogenic acid can inhibit the release of inflammatory mediators such as NO, TNF-*α*, and IL-6 in LPS-induced RAW 264.7 macrophages. Consequently, the anti-inflammatory activity of compound **1** was significantly greater than that of other compounds (Hwang et al. 2014). To gain initial insights into its molecular mechanism beyond the phenotypic NO assay, we performed *in silico* molecular docking simulations. The results showed that methyl chlorogenate possesses a high predicted binding affinity for the pro-inflammatory cytokine TNF-α, forming stable interactions within its active site. TNF-α is a master regulator of the inflammatory cascade. Its inhibition is a validated therapeutic strategy for several inflammatory diseases. This computational evidence provides a plausible and direct mechanistic hypothesis: the anti-inflammatory efficacy of compound **1** observed in our cellular model may be mediated, at least partially, through the direct antagonism of TNF-α activity, thereby disrupting the downstream inflammatory signal transduction (Li et al. 2022). While this requires experimental validation through methods such as SPR or functional TNF-α inhibition assays, the docking study offers a valuable directional clue for future mechanistic research. In conclusion, this study moves beyond the root-centric paradigm of *B. chinense* research by establishing its aerial parts as a chemically distinct and bioactive fraction. The isolation and bioactivity assessment of

isolated compounds as potent anti-inflammatory agents underscore the potential of this understudied plant material in drug discovery. The proposed mechanism involving TNF-α interaction, derived from molecular docking, sets a clear foundation for subsequent *in vitro* and *in vivo* studies to fully elucidate its mode of action and therapeutic potential.

CONCLUSION

16 compounds were successfully extracted and isolated from the aerial parts of *B. chinense*. Structural elucidation was accomplished through a combination of MS and NMR. Anti-inflammatory activity studies were conducted on these **16** compounds. Methyl chlorogenate (Compound **1**) exhibited the most marked inhibition of LPS-triggered NO production in RAW 264.7 macrophages, with several other compounds also displaying significant anti-inflammatory activity. Overall, these findings contribute to clarifying the anti-inflammatory active compounds in the aerial parts of *B. chinense*. More importantly, this study enriched the chemical composition of the aerial parts of *B. chinense* and also showed the potential mechanism of its anti-inflammatory effect through molecular docking technology. It provided new ideas and methods for the modernization research of traditional Chinese medicine resources.

ACKNOWLEDGEMENTS

This work was funded by the Project of Science and Technology Department of Liaoning province (2023JH2/101600021), the Excellent Youth Promotion Project of Shenyang University of Chemical Technology (2022YQ008), Young and Middle-aged Scientific and Technological Innovation Talents in Shenyang of Liaoning province (RC210148), the Project of Education Department of Liaoning Province (LJ212410149033, LJ232410149068, LJ232510149002), National-Local Joint Engineering Laboratory for Development of Boron and Magnesium Resources and Fine Chemical Technology (LJ232410149002). All supplementary data is available upon requests from the corresponding author.

REFERENCES

Asamenew, G., Kim, H.W., Lee, M.K., Lee, S.H., Lee, S., Cha, Y.S., Lee, S.H., Yoo, S.M. & Kim, J.B. 2019 Comprehensive characterization of hydroxycinnamoyl derivatives in green and roasted coffee beans: A new group of methyl hydroxycinnamoyl quinate. *Food Chemistry X* 2: 100033.

Conradt, D., Hermann, B., Gerhardt, S., Einsle, O. & Müller, M. 2016. Biocatalytic properties and structural analysis of phloroglucinol reductases. *Angewandte Chemie* 55(50): 15531-15534.

Deng, W-F., He, J-L., Zhu, Y-D., Deng, C-F. & Nan, Z-D. 2024. Chemical constituents from the aerial parts of *Corydalis fangshanensis* and their inhibitory effects on breast cancer cells proliferation. *Journal of Natural Products Research and Development* 36(2): 252-259.

Fan, Y.X., Ma, Y.G., Zhu, Y.J., Xin, J.L., Dai, X.Y., Du, K., Cao, Y.G., Sun, Y.J., Zheng, X.K., Feng, W.S. & Chen, H. 2025. Phenylpropanoid glycosides from the fruits of *Lycium chinense* and their potential anti-diabetic activity. *Fitoterapia* 187: 106878.

Hwang, S.J., Kim, Y.W., Park, Y., Lee, H.J. & Kim, K.W. 2014. Anti-inflammatory effects of chlorogenic acid in lipopolysaccharide-stimulated RAW 264.7 cells. *Inflammation Research* 63(1): 81-90.

Intaraudom, C., Bunbamrung, N., Dramae, A., Boonyuen, N., Kongsaeree, P., Srichomthong, K., Supothina, S. & PittayakhaJonwut, P. 2017. Terphenyl derivatives and drimane - Phathalide/isoindolinones from *Hypoxylon fendleri* BCC32408. *Phytochemistry* 139: 8-17.

Liao, H., Liu, H. & Yuan, K. 2012. A new flavonol glycoside from the *Abelmoschus esculentus* Linn. *Pharmacognosy Magazine* 8(29): 12-15.

Liu, C.P., Liu, J.X., Gu, J., Liu, F., Li, J.H., Bin-Yang, Yuan-Zheng, Jie-Li, Wu, S., Wu, Q., Xian-Zhang, Li, L.M., Yang, H.L., Wang, L. & Li, X. 2021. Combination effect of three main constituents from *Sarcandra glabra* inhibits oxidative stress in the mice following acute lung injury: A role of MAPK-NF-κB pathway. *Frontiers in Pharmacology* 11: 580064.

Li, H., Pan, S. & Xu, X. 2019. Structure characteristics of flavonoids for cyclooxygenase-2 mRNA inhibition in lipopolysaccharide-induced inflammatory macrophages. *European Journal of Pharmacology* 856: 172416.

Li, M., Chi, J., Zhang, W-J., Wang, Z-M. & Dai, L-P. 2024. Study on the chemical constituents from ethyl acetate extract of *Ipomoea turbinata* seeds. *Journal of Natural Products Research and Development* 36(9): 1528-1536.

Li, X., Liu, Y., Wang, S., Guan, W., Pan, J., Kuang, H. & Yang, B. 2022. Identification and potential mechanism of different components from the aerial part of *B. chinense* for epileptic treatment. *Natural Product Research* 36(23): 6137-6142.

Ma, X., Dang, C., Kang, H., Dai, Z., Lin, S., Guan, H., Liu, X., Wang, X. & Hui, W. 2015 Saikosaponin-D reduces cisplatin-induced nephrotoxicity by repressing ROS-mediated activation of MAPK and NF-κB signalling pathways. *International Immunopharmacology* 28(1): 399-408.

Navarro, P., Giner, R.M., Recio, M.C., Máñez, S., Cerdá-Nicolás, M. & Ríos, J.L. 2001. *In vivo* anti-inflammatory activity of saponins from *Bupleurum rotundifolium*. *Life Sciences* 68(10): 1199-1206.

Park, W.H., Kang, S., Piao, Y., Pak, C.J., Oh, M.S., Kim, J., Kang, M.S. & Pak, Y.K. 2015 Ethanol extract of *Bupleurum falcatum* and saikosaponins inhibit neuroinflammation via inhibition of NF-κB. *Journal of Ethnopharmacology* 174: 37-44.

Pel, P., Chae, H.S., Nhoek, P., Kim, Y.M., An, C.Y., Yoo, H., Kang, M., Kim, H.W., Choi, Y.H. & Chin, Y.W. 2022. Chemical constituents from the roots and rhizomes of *Sophora tonkinensis* and their effects on proprotein convertase substilisin/kexin type 9 expression. *ACS Omega* 7(24): 20952-20958.

Que, D.M., Dai, H.F. & Huang, G.X. 2009. Chemical constituents from the endophytic fungus *Rhizoctonia* sp. J5 of *Antiaris toxicaria*. *Journal of Natural Products Research and Development* 21(3): 424-427.

Shrestha, S., Lee, D.Y., Park, J.H., Cho, J.G., Lee, D.S., Li, B., Kim, Y.C., Kim, G.S., Bang, M.H. & Baek, N.I. 2013. Phenolic components from *Rhus parviflora* fruits and their inhibitory effects on lipopolysaccharide-induced nitric oxide production in RAW 264.7 macrophages. *Natural Product Research* 27(23): 2244-2247.

Sun, P., Li, Y., Wei, S., Zhao, T., Wang, Y., Song, C., Xue, L., Wang, F., Xiao, L., Wu, J. & Qiao, M. 2019. Pharmacological effects and chemical constituents of *Bupleurum*. *Mini Reviews in Medicinal Chemistry* 19(1): 34-55.

Takara, K., Matsui, D., Wada, K., Ichiba, T. & Nakasone, Y. 2002. New antioxidative phenolic glycosides isolated from Kokuto non-centrifuged cane sugar. *Bioscience, Biotechnology, and Biochemistry* 66(1): 29-35.

Tazaki, H., Ito, M., Miyoshi, M., Kawabata, J., Fukushi, E., FuJita, T., Motouri, M., Furuki, T. & Nabeta, K. 2002. Subulatin, an antioxidic caffeic acid derivative isolated from the *in vitro* cultured liverworts, *Jungermannia subulata, Lophocolea heterophylla*, and *Scapania parvitexta*. *Bioscience Biotechnology and Biochemistry* 66(2): 255-261.

Torres-Rodríguez, M.L., García-Chávez, E., Berhow, M. & de Mejia, E.G. 2016. Anti-inflammatory and anti-oxidant effect of *Calea urticifolia* lyophilized aqueous extract on lipopolysaccharide-stimulated RAW 264.7 macrophages. *Journal of Ethnopharmacology* 188: 266-274.

Wen, Q., Lin, X., Liu, Y., Xu, X., Liang, T., Zheng, N., Kintoko, & Huang, R. 2012. Phenolic and lignan glycosides from the butanol extract of *Averrhoa carambola* L. root. *Molecules* (Basel, Switzerland) 17(10): 12330-12340.

Yan, M., Zhang, D. & Yang, M. 2024. Saikosaponin D alleviates inflammatory response of osteoarthritis and mediates autophagy via elevating microRNA-199-3p to target transcription Factor-4. *Journal of Orthopaedic Surgery and Research* 19(1): 151.

Yang, F., Dong, X., Yin, X., Wang, W., You, L. & Ni, J. 2017. *Radix Bupleuri*: A review of traditional uses, botany, phytochemistry, pharmacology, and toxicology. *BioMed Research International* 2017: 7597596.

Yang, S.Y., Lin, Z.X., Xian, Y.F., Zhang, H.M. & Xu, H.X. 2023. Traditional uses, chemical compounds, pharmacological activities and clinical studies on the traditional Chinese prescription Yi-Gan San. *Journal of Ethnopharmacology* 302(Pt A): 115859.

Yang, Y., Chen, H., Sun, J., Chen, Y., Bai, D., Wang, S., Zhang, J., Song, J., Sun, Z. & Dai, L. 2025. Research progress on extraction, purification, biotransformation, pharmacological effects, toxicity, combined therapy and new dosage forms of saikosaponins. *Journal of Ethnopharmacology* 352: 120274.

Yang, X., Zhang, C., Wu, Z., Zhang, P., Zhao, M., Jiang, Y., & Tu, P. 2018. Sesquiterpenes from Artemisia giraldii var. longipedunculata. *Journal of Chinese Pharmaceutical Sciences* 27(8): 576–581.

Zhang, L., Fan, Y., Su, H., Wu, L., Huang, Y., Zhao, L., Han, B., Shu, G., Xiang, M. & Yang, J.M. 2018. Chlorogenic acid methyl ester exerts strong anti-inflammatory effects via inhibiting the COX-2/NLRP3/NF-κB pathway. *Food & Function* 9(12): 6155-6164.

Zhao, M., Xiao, L., Chen, Q., Shen, L., Zhao, G., Linghu, K., Ma, Q., Dar, P. & Yu, H. 2025 Bioactive equivalent combinatorial compounds contributing to the holistic effect of traditional Chinese medicine *Bupleuri chinense* DC. *Journal of Ethnopharmacology* 350: 120003.

*Corresponding author; email: lidanqi@yeah.net